

Trapped fermionic clouds distorted from the trap shape due to many-body effects

Masudul Haque^{1,2} and H. T. C. Stoof²

¹*Max Planck Institute for Physics of Complex Systems, Dresden, Germany*

²*Institute for Theoretical Physics, Utrecht University,
Leuvenlaan 4, 3584 CE Utrecht, The Netherlands*

(Dated: May 22, 2018)

We present a general approach for describing trapped Fermi gases, when the cloud shape is distorted with respect to the trap shape. Our approach provides a consistent way to explore physics beyond the local density approximation, if this is necessary due to the distortion. We illustrate this by analyzing in detail experimentally observed distortions in a trapped imbalanced Fermi mixture. In particular, we demonstrate in that case dramatic deviations from ellipsoidal cloud shapes arising from the competition between surface and bulk energies.

Introduction. — The cooling of trapped fermionic atoms to degeneracy has opened up a fascinating new arena for studying many-fermion physics [1]. In particular, the opportunity to access the BEC-BCS crossover using Feshbach resonances has led to a large effort in the experimental study of fermionic pairing using trapped atomic gases [2]. Among other topics, pairing in polarized Fermi gases is now being intensely explored, experimentally in Refs. [3, 4, 5, 6] and theoretically in, e.g., Refs. [7, 8, 9, 10, 11, 12]. Apart from possible new insights for solid-state and nuclear physics, the field of trapped fermionic atoms comes with its own set of new concerns, such as the role of the trapping potential. In this Letter, we therefore provide results on the relationship between the trap shape and the shape of the gas cloud.

For a large class of trapped many-body systems, the local density approximation (LDA) gives an accurate description of the spatial distributions of atomic and energy densities. However, motivated by recent experiments [4, 6], we propose that a number of mechanisms may lead to the intriguing situation that the combination of many-body physics and the external trapping potential causes the shape of the gas cloud to be distorted compared to the shape determined by the trap alone. In such cases, the simple LDA procedure in terms of a local chemical potential is no longer appropriate, and we need to consider the angular structure of the local Fermi surface. We have therefore formulated an extension of the LDA that allows for a distinction between the different directions. We give below some examples where one observes or expects such spatial distortions. We note however that there might be many other situations, beyond what we anticipate here, where such distortions take place. Our formalism is thus of very general applicability and interest.

As a first scenario for spatial distortions, consider a many-body system that is phase separated in an elongated trap due to the presence of a first-order transition. The interface between the two phases then carries a surface tension. To minimize the surface energy, the interface shape will differ from the trap shape. In fact, such a system has recently been experimentally realized

using a trapped polarized Fermi mixture of resonantly-interacting atoms [4, 6]. At sufficiently low temperatures this mixture phase separates into an unpolarized superfluid core and an outer shell of normal polarized fermions [4, 7, 8, 9, 10, 11]. When the trap is elongated enough and the particle number is small enough, the surface tension causes significant deviation of the core aspect ratio from the trap aspect ratio [6, 12]. In the following we will analyze this situation in detail.

Second, Pomeranchuk instabilities are shape deformation instabilities of a Fermi surface [13], which have attracted intense interest in the strongly correlated electrons community [14, 15]. A *d*-wave Pomeranchuk transition leads to a “nematic” Fermi liquid with an elliptical Fermi surface. Other than their possible realization in solids, it is hoped that such a nematic liquid may be realized in atomic dipolar Fermi gases since a long-range interaction can cause a Pomeranchuk instability if the short-range part is suppressed [15]. A Fermi surface deformation that is constant in space causes no distortion in coordinate space. However, in an external trap, the Fermi surface deformation would vary from point to point, leading to a distortion of the gas cloud in coordinate space as well. To calculate particle and energy densities in such a case, would again require an anisotropic generalization of the LDA, of the kind we provide here.

Finally, one possible mechanism for pairing of polarized fermions is via opposite deformation of the two Fermi surfaces [16]. A prolate (oblate) shape for the majority (minority) Fermi surface leads to an equatorial region in momentum space along which opposite-momenta fermions can pair. With the extended parameter space expected to be accessible with trapped atoms in the future, it is likely that this pairing mechanism is energetically favorable in some parameter regime [16]. In the case of such pairing in a trap, we expect both Fermi surfaces to have ellipticities (of opposite sign) that vary with position. As a result, the majority and minority clouds are expected to be distorted in opposite directions relative to the trap. Again, a treatment of the type presented in this Letter is needed to describe this situation.

Anisotropic generalization of local density approxima-

tion— The LDA encodes the inhomogeneity of the gas completely in terms of a local chemical potential at every point in space, $\mu(\mathbf{r}) = \mu - V_{\text{tr}}(\mathbf{r})$. Here μ is the true chemical potential of the gas and $V_{\text{tr}}(\mathbf{r})$ is the trapping potential. The shape of the gas cloud is determined by an equipotential surface of the trap. For harmonic traps, this surface is an ellipsoid.

The key to treating distorted systems is to generalize the definition of the local chemical potential $\mu(\mathbf{r}) = \mu - V_{\text{tr}}(\mathbf{r})$ in a way that discriminates between directions. For definiteness, we will consider axially symmetric traps, $V_{\text{tr}}(\mathbf{r}) = V_{\text{tr}}(r, z)$, where r and z are the radial and axial length variables of a cylindrical coordinate system, respectively. For each position in the trap, we need to determine the momentum-space location of the deformed Fermi surface, in both the radial and axial directions. We denote by $R(z)$ and $Z(r)$ the edge of a reference ideal Fermi cloud, that would be obtained by hypothetically turning off the interactions but retaining the distortion. Our prescriptions for the location of the Fermi surface at position \mathbf{r} in the radial and axial directions are

$$\mu_{\text{R}}(\mathbf{r}) = \mu_{\text{R}}(r, z) = V_{\text{tr}}(R(z), z) - V_{\text{tr}}(r, z), \quad (1a)$$

$$\mu_{\text{Z}}(\mathbf{r}) = \mu_{\text{Z}}(r, z) = V_{\text{tr}}(r, Z(r)) - V_{\text{tr}}(r, z). \quad (1b)$$

We have written the Fermi surface locations in energy units, i.e., μ_{R} and μ_{Z} are the free-particle energies corresponding to the Fermi momenta in the radial and axial directions. They are, of course, not components of the chemical potential. Eqs. (1) are obtained by semiclassical considerations similar to the WKB approximation, which is one way to derive the LDA. Here, we have applied the semiclassical approximation separately to the r and z directions (Fig. 1a) as appropriate for an axially symmetric trap, where the single-particle Schrödinger equation separates in these two directions.

After obtaining the locations of the local Fermi surface in the radial and axial directions, it is for many purposes sufficient to use an ellipsoidal Fermi surface with μ_{R} and μ_{Z} as the principal axes. At the center of the trap, the same semiclassical argument can be carried out in any direction and the local Fermi surface has exactly the same shape as the edge of the ideal gas reference cloud. The cloud shape is generally near ellipsoidal but may deviate from this shape either due to anharmonicity of the trap or due to many-body effects, as we will see. Although the shape of the Fermi surface away from the trap center is not fixed by similar arguments, it is physically reasonable to use the same shape as in the trap center.

The local non-spherical Fermi surfaces obtained using this prescription can now be used to calculate densities. For example, for an elliptically distorted normal gas in a harmonic trap, the density is given in terms of the volume of the local Fermi surface by $n(\mathbf{r}) = [(2m)^{3/2}/6\pi^2] \mu_{\text{R}}(\mathbf{r})\sqrt{\mu_{\text{Z}}(\mathbf{r})}$. This density vanishes at the surface defined by $R(z)$ or $Z(r)$. For a superfluid, on

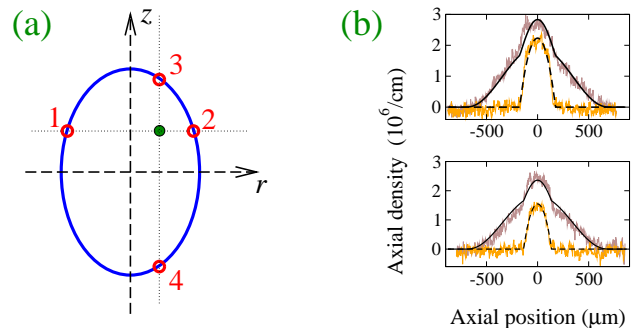


FIG. 1: (Color online.) (a) Calculation of the local anisotropic Fermi surface at position \mathbf{r} (full dot). Points 1 and 2 with coordinates $(\pm R(z), z)$ are the classical turning points for the motion in the r -direction. Points 3 and 4, i.e., $(r, \pm Z(r))$, are the classical turning points for motion in the z direction. (b) Fits to the axial density profiles for both species using our approach. The top and bottom panels show two experimental shots, at polarizations $P \simeq 0.5$ and $P \simeq 0.65$, respectively.

the other hand, it may be appropriate to use the BCS equations generalized to anisotropic Fermi surfaces, i.e., the momentum integrand in the density profile

$$n(\mathbf{r}) = \int_0^\infty \frac{k^2 dk}{2\pi^2} \int_{-1}^1 dx \left(1 - \frac{\epsilon_{\mathbf{k}} - \epsilon_{\text{F}}(x)}{\sqrt{[\epsilon_{\mathbf{k}} - \epsilon_{\text{F}}(x)]^2 + |\Delta|^2}} \right)$$

now has angular dependence. Here $x = \cos\theta$, $\epsilon_{\mathbf{k}} = \hbar^2 \mathbf{k}^2 / 2m$ with m the atomic mass, Δ is the gap, and $\epsilon_{\text{F}}(x)$ is the deformed Fermi surface with principal axes μ_{R} and μ_{Z} . Similar modifications can be made for the BCS energy equation and the BCS gap equation.

Application to polarized resonantly-interacting Fermi gases — We now demonstrate our procedure by elaborating on a particular case, i.e., we analyze the experiment reported in Ref. [6] using the formalism presented above. Figure 2 of Ref. [6] shows that the majority aspect ratio does not change much with polarization. We therefore describe the majority species in state $|\uparrow\rangle$ with the usual LDA. On the other hand, the boundary of the minority atom cloud in state $|\downarrow\rangle$ is distorted due to surface tension. We thus treat the minority according to the approach described above. At each position within the minority cloud, we calculate the two parameters for the Fermi surface of the minority species, using as an input the boundary of the minority cloud, which coincides with the superfluid core if any intermediate partially-polarized normal shell can be neglected.

For a choice of μ_{\uparrow} , $R_{\downarrow} \equiv R_{\downarrow}(0)$, and $Z_{\downarrow} \equiv Z_{\downarrow}(0)$, the particle densities $n_{\uparrow}(\mathbf{r}) = n_{\downarrow}(\mathbf{r})$ and the energy density $e(\mathbf{r})$ at any point inside the core can be calculated from the local Fermi surfaces. The majority Fermi surface is given by $\mu_{\uparrow}(\mathbf{r}) = \mu_{\uparrow} - V_{\text{tr}}(\mathbf{r})$. The minority Fermi surface is deformed, with $\mu_{\text{R}\downarrow}(\mathbf{r})$ and $\mu_{\text{Z}\downarrow}(\mathbf{r})$ calculated using Eqs. (1). Since at resonance the gap is larger than

the maximum difference between the Fermi surfaces, the minority momentum distribution is not anisotropic even though $\mu_{R\downarrow} \neq \mu_{Z\downarrow}$, unlike the case of Refs. [16]. For the fully polarized normal gas outside the core, $n_{\uparrow}(\mathbf{r})$ and $e(\mathbf{r})$ are calculated by the usual LDA.

To calculate the densities and superfluid gap in the superfluid core, we could use generalized BCS equations as described above. However, with one additional approximation, we can also make use of Monte Carlo results [17] for the resonant situation near which the experiments of Refs. [4, 6] are performed. The additional approximation is to use at every position an effective chemical potential $\mu_{\downarrow}(\mathbf{r}) = [\mu_{R\downarrow}(\mathbf{r})]^{2/3}[\mu_{Z\downarrow}(\mathbf{r})]^{1/3}$ for the minority species as well. The superfluid properties are then given by the universal unitarity results [17] in terms of the average chemical potential $\mu(\mathbf{r}) = [\mu_{\downarrow}(\mathbf{r}) + \mu_{\uparrow}(\mathbf{r})]/2$.

In Fig. 1b, we show the resulting axial density profiles, and compare with experimental data for two different polarizations $P = (N_{\uparrow} - N_{\downarrow})/(N_{\uparrow} + N_{\downarrow})$. The calculation requires three parameters (μ_{\uparrow} , R_{\downarrow} , Z_{\downarrow}) as input. Unlike the calculation in Ref. [10], the required input quantities are not immediately fixed by the trap parameters and particle numbers ($N_{\uparrow}, N_{\downarrow}$) alone. An additional energy calculation is required for the aspect ratio of the core, as explained later. The experimental majority axial density profiles have pronounced peaks at the center. This is reproduced well by the calculations shown in Fig. 1 using Monte Carlo unitarity parameters, but not if we use the BCS equations to describe the core. Note that these central peaks are not prominent in the first experiment by Partridge *et al.* [4], nor in the experiment by Shin *et al.* [5], suggesting that thermal fluctuations play a stronger role in those cases. In all calculations reported in this Letter, anharmonicities of the experimental trap shape are included unless explicitly stated otherwise.

Energy minimization — At unitarity, the surface energy density associated with the superfluid-normal interface is expected to be given by the chemical potentials through universal constants. Defining $\mu = (\mu_{\uparrow} + \mu_{\downarrow})/2$ and $h = (\mu_{\uparrow} - \mu_{\downarrow})/2$, we first note that a quantity with the dimension of a surface energy density constructed out of μ alone must be proportional to $(m/\hbar^2)\mu^2$. The dependence on h may be included as a function of the dimensionless ratio h/μ . The surface tension thus has the form $\sigma = \eta_s(m/\hbar^2)\mu^2 f_s(h/\mu)$. Here η_s is a dimensionless number expected to be of order 1 and f_s is a dimensionless function. Noting in addition that the position of the interface is fixed by the first-order transition determined by a universal value of h/μ [17], we infer that $f_s(h/\mu)$ is a constant along the surface we are interested in. We thus absorb it into the universal constant η_s .

We can use the observed core aspect ratios $Z_{\downarrow}/R_{\downarrow}$ extracted from the axial density data to determine η_s , because the correct value of η_s must produce a total energy minimum at the correct aspect ratio. Denoting by $n_N(\mu)$ and $e_N(n)$ the particle and energy-density

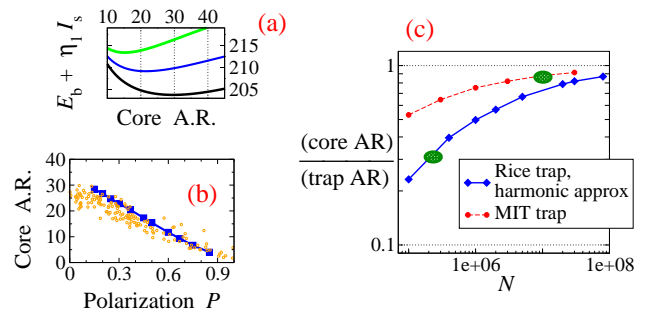


FIG. 2: (Color online.) (a) Total energy curves for fixed $(N_{\uparrow}, N_{\downarrow}) = (194, 92.7) \times 10^3$, shown for η_s values of 0.30, 0.59 and 0.90 from bottom to top. (b) Core aspect ratio (A.R.) as a function of polarization for $N_{\uparrow}/10^3 = 200 - 80P$ and calculated with $\eta_s = 0.6$. (c) Core A.R. versus particle number, for fixed polarization $P = 0.49$. The regions relevant to experiments [3, 4, 5, 6] are indicated by shaded ellipses.

functions of a homogeneous two-component ideal Fermi gas, the bulk energy density in the superfluid core is given by $e(\mathbf{r}) = (1 + \beta)e_N(n(\mathbf{r})) + V_{\text{tr}}(\mathbf{r})n(\mathbf{r})$, where $n(\mathbf{r}) = n_N(\mu(\mathbf{r})/(1 + \beta))$ is the density profile in the core, $\beta \simeq -0.585$ is a universal constant [17], and $\mu(\mathbf{r})$ is calculated as described previously. The energy density in the outer shell is given simply by the single-component ideal Fermi gas expression. Integrating over the core and the outer shell gives the total bulk energy E_b .

The total energy is $E_b + \eta_s I_s$, where I_s is the surface integral over $(m/\hbar^2)\mu^2(\mathbf{r})$. In Fig. 2a, this quantity is shown for several values of η_s , for fixed populations. The axial data in an experimental shot for these populations is fit well with $Z_{\downarrow}/R_{\downarrow} \simeq 21.5$ and a minimum is located at this core aspect ratio for $\eta_s \simeq 0.59$. Carrying out this procedure with several experimental axial density profiles, we obtain the estimate $\eta_s = 0.60 \pm 0.15$. The error bar leads to uncertainties in the calculated aspect ratios that is about 2% for the smallest deformations and about 10% for the largest deformations.

Variation of core deformation — Having determined the universal constant η_s , we can compare our theory to the experimental core aspect ratio versus polarization curve in Figure 2 of Ref. [6]. The aspect ratio actually depends on the total particle number in addition to the polarization. In the experiment, there are shot-to-shot variations of N_{\uparrow} and a systematic bias towards larger N_{\uparrow} at smaller P . We model this bias as $N_{\uparrow} = (200 - 80P) \times 10^3$. Most of the shots are scattered around this line. Our results are shown in Fig. 2b, together with the experimental data.

In Fig. 2c, we display the core deformation as a function of total particle number. Surface effects are less important in the thermodynamic limit $N \rightarrow \infty$ and the difference between core and trap aspect ratios vanishes as $N^{-1/3}$ in this limit [12]. The lower curve is for a harmonic trap matching the trap of Ref. [6] at the center.

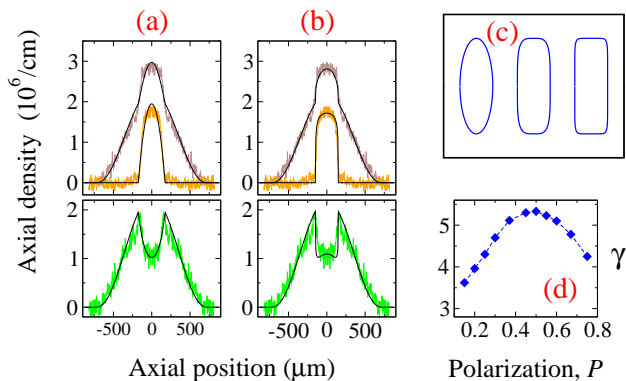


FIG. 3: (Color online.) Experimental axial density curves fitted with core shapes (a) $\gamma = 2$ and (b) $\gamma = 8$. Top panels show species axial densities, bottom panels show difference. The value $\gamma = 2$ misses the “flat” features, while $\gamma = 8$ over-emphasizes them. (c) Surface shapes for $\gamma = 2, 4$, and 9 , respectively. (d) Calculated value of γ for various polarizations, along the line $N_{\uparrow}/10^3 = 200 - 80P$.

The upper curve presents our expected result for the experiments of Shin *et al.* [5]. The predicted deformation of about 10% appears to be sufficiently large to have been observable in these experiments, which is consistent with the interpretation of Gubbels *et al.* [18] that no phase separation has occurred in this case.

Deviation from ellipsoidal shape — Examination of the high-polarization data of Figure 1 of Ref. [6] reveals a peculiar feature. The minority absorption images, other than having a lower aspect ratio than the trap, also have shapes that are not quite ellipsoidal and tend to be somewhat cylindrical. The axial density profiles reveal the same geometric effect in terms of flatter peaks than would be expected for an ellipsoidal shape. Our formalism is well-suited for studying this effect, since the core boundary simply translates into distortions of local Fermi surfaces that can be used to calculate consistent density and energy profiles. We parameterize non-elliptical shapes by describing the core surface by the equation $(r/R)^\gamma + (z/Z)^\gamma = 1$. Using a γ equal to 2 gives an ellipsoid and infinite γ gives a cylinder. Comparing axial density profiles obtained with various values of γ , as in Figs. 3a and 3b, shows that the experimental features, e.g. the flat tops, are best reproduced with γ between 3 and 6, with the best γ tending to increase with increasing polarization, up to about $P \simeq 0.6$. However, a precise determination of γ is difficult from these fits alone.

Our formalism also allows us to extract γ from an energy calculation. Minimizing the total (bulk plus surface) energy, under the constraint of constant particle numbers, produces the observed deviation from ellipsoidal shape, with $\gamma > 2$ and γ increasing with P for moderate polarizations (Fig. 3d). The energy calculation also predicts a decrease of γ at larger P . This prediction is difficult to verify from the currently available axial den-

sity data because of the large fluctuations of $(N_{\uparrow}, N_{\downarrow})$ from the line $N_{\uparrow}/10^3 = 200 - 80P$.

Conclusions — To summarize, we have presented an anisotropic extension of the local density approximation in order to deal with situations where the aspect ratio of trapped fermionic gases differs from the trap aspect ratio due to many-body effects. Our procedure allows for a consistent calculation of the density and energy profiles. We have demonstrated this via a detailed analysis of experiments with phase-separated polarized fermions.

In particular, we have uncovered and explained a striking new effect concerning the shape of the superfluid core, which takes an unexpected non-ellipsoidal form. Our treatment dramatically highlights the utility of our formulation: we know of no other way of calculating the density distributions for an arbitrary cloud shape.

Acknowledgments — We benefited greatly from discussions and collaboration with the experimental group at Rice University, in particular Wenhui Li and Randy Hulet.

-
- [1] B. DeMarco and D. S. Jin, *Science* **285**, 1703 (1999); A. G. Truscott *et al.*, *Science* **291**, 2570 (2001); F. Schreck *et al.*, *Phys. Rev. Lett.* **87**, 080403 (2001);
 - [2] C. A. Regal, M. Greiner, and D. S. Jin, *Phys. Rev. Lett.* **92**, 040403 (2004); M. W. Zwierlein *et al.*, *Phys. Rev. Lett.* **92**, 120403 (2004); M. Bartenstein *et al.*, *Phys. Rev. Lett.* **92**, 120401 (2004).
 - [3] M. W. Zwierlein, A. Schirotzek, C. H. Schunck, and W. Ketterle, *Science* **311**, 492 (2006).
 - [4] G. B. Partridge, W. Li, R. I. Kamar, Y. A. Liao, and R. G. Hulet, *Science* **311**, 503 (2006).
 - [5] Y. Shin, M. W. Zwierlein, C. H. Schunck, A. Schirotzek, and W. Ketterle, *Phys. Rev. Lett.* **97** 030401 (2006).
 - [6] G. B. Partridge, W. Li, Y. A. Liao, and R. G. Hulet, M. Haque and H. T. C. Stoof, *Phys. Rev. Lett.* **97**, 190407 (2006).
 - [7] D. E. Sheehy and L. Radzihovsky, *Phys. Rev. Lett.* **96**, 060401 (2006).
 - [8] H. Caldas, *Phys. Rev. A* **69**, 063602 (2004).
 - [9] F. Chevy, *Phys. Rev. Lett.* **96**, 130401 (2006).
 - [10] M. Haque and H. T. C. Stoof, *Phys. Rev. A* **74**, 011602(R) (2006).
 - [11] T. N. De Silva and E. J. Mueller, *Phys. Rev. A* **73**, 051602(R) (2006).
 - [12] T. N. De Silva and E. J. Mueller, *Phys. Rev. Lett.* **97**, 070402 (2006).
 - [13] I. Ia. Pomeranchuk, *JETP* **35**, 524 (1958).
 - [14] V. Oganesyan, S. A. Kivelson, and E. Fradkin, *Phys. Rev. B* **64**, 195109 (2001). W. Metzner, D. Rohe, and S. Andergassen; *Phys. Rev. Lett.* **91**, 066402 (2003).
 - [15] J. Quintanilla and A. J. Schofield, *Phys. Rev. B* **74**, 115126 (2006).
 - [16] H. Müther and A. Sedrakian, *Phys. Rev. Lett.* **88**, 252503 (2002); A. Sedrakian, I. J. Mur-Petit, A. Polls, and H. Müther, *Phys. Rev. A* **72**, 013613 (2005).
 - [17] J. Carlson and S. Reddy, *Phys. Rev. Lett.* **95**, 060401 (2005).

- [18] K. B. Gubbels, M. W. J. Romans, and H. T. C. Stoof,
Phys. Rev. Lett. **97**, 210402 (2006).